Nuclear Theory'22
ed. V. Nikolaev, Heron Press, Sofia, 2003

Relativistic model of electromagnetic one-nucleon knockout reactions

F. D. Pacati, C. Giusti, and A. Meucci

Dipartimento di Fisica Nucleare e Teorica dell'Università degli Studi di Pavia and Istituto Nazionale di Fisica Nucleare, Sezione di Pavia, Italy

Abstract.

A relativistic model of electromagnetic knockout emission is presented and applied to $(e, e'p)$ and (γ, p) cross sections and polarizations. The results are compared with those obtained in the nonrelativistic distorted wave impulse approximation, which is able to well reproduce the experimental data at low energies. The effect of two-body currents, including meson exchange contributions and isobar excitations, is discussed both in the relativistic and nonrelativistic framework.

1 Introduction

One-nucleon knockout reactions represent a clean tool to explore the single-particle aspects of nuclei revealing the properties of their hole states [1–4].

Several high-resolution $(e, e'p)$ experiments were carried out at Saclay [1, 5] and NIKHEF [6]. The analysis of the experimental cross sections allowed to describe, with a high degree of accuracy, in a wide range of nuclei and in different kinematics, the shape of the experimental momentum distributions at missing-energy values corresponding to specific peaks in the energy spectrum and to assign specific spectroscopic factors to these peaks. The calculations were carried out within the theoretical framework of a nonrelativistic distorted wave impulse approximation (DWIA), where final-state interactions and Coulomb distortion of the electron wave functions are taken into account [7].

New data have recently become available from TJNAF. The cross section has been measured and the response functions have been extracted in the ^{16}O$(e, e'p)$ reaction at four-momentum transfer squared $Q^2 = 0.8$ (GeV/c)^2 and energy

transfer $\omega \sim 439$ MeV [8]. In the same kinematics also first polarization transfer measurements have been carried out for the ^{16}O$(\vec{e}, e'\vec{p})$ reaction [9]. The polarization of the ejected proton in the ^{12}C$(e, e'\vec{p})$ reaction has been measured at Bates with $Q^2 = 0.5$ (GeV/c)^2 and outgoing-proton energy $T_{\rm p} = 274$ MeV [10].

The analysis of these new data in kinematic conditions inaccessible in previous experiments, where Q^2 was less than 0.4 (GeV/c)^2 and $T_{\rm p}$ generally around 100 MeV, requires a theoretical treatment where all relativistic effects are carefully included. A fully relativistic model is therefore needed. It is thus important to compare the nonrelativistic DWIA treatment that was extensively used in the analysis of low-energy data, with the relativistic DWIA (RDWIA) treatment, in order to understand the limit of validity of the nonrelativistic model.

The nonrelativistic approach is briefly outlined in Section 2. The relativistic formalism is given in Section 3, where the results obtained are compared with the experimental data and the nonrelativistic calculations. The effect of meson-exchange current contributions both in the nonrelativistic and in the relativistic model is presented in Section 4. Some conclusions are drawn in Section 5.

2 Nonrelativistic Model

In the one-photon exchange approximation, the coincidence cross section of the $(e, e'p)$ reaction is given in plane wave impulse approximation by the factorized formula:

$$\sigma_0 = K \sigma_{\rm ep} S(E, \boldsymbol{p}) \, , \tag{1}$$

where K is a kinematic constant, $\sigma_{\rm ep}$ the off-shell electron-proton cross section, and $S(E, \boldsymbol{p})$ the spectral density function, which gives the joint probability to find in the target nucleus a proton with energy E and momentum $\boldsymbol{p}$.

In order to take into account the final-state interaction of the outgoing proton with the nucleus, the scattering wave functions are calculated as eigenfunctions of an energy-dependent optical potential determined through a fit to elastic proton-nucleus scattering data. In this case the cross section σ_0 is no more factorized [3].

The bound-state wave functions are obtained from a single-particle potential, where the radius is determined to fit the experimental momentum distributions and the depth is adjusted to give the experimentally observed separation energies.

The nuclear current contains in addition to the charge contribution, the convective and the spin components. The nucleon form factors are taken in the on-shell form, even if the initial nucleon is off-shell. Some relativistic corrections are included, obtained from the Foldy-Wouthuysen reduction of the free-nucleon Dirac current, through an expansion in a power series of the inverse nucleon mass, truncated at second order.

Current conservation is restored by replacing the longitudinal current, with respect to momentum transfer $\boldsymbol{q}$, by

$$J^{\mathrm{L}} = \frac{\omega}{q} J^0 \ . \tag{2}$$

The nonrelativistic model was able to provide a good description of experimental data over a wide kinematic range, corresponding to a kinetic energy of the outgoing proton around 100 MeV, and for a number of nuclei with different mass from ^{12}C to ^{208}Pb [3]. The spectroscopic factors, obtained from the comparison between the theoretical calculations and the experimental data, were much smaller than expected from the independent particle model [3], addressing to nuclear correlations.

3 Relativistic Model

In RDWIA the matrix elements of the nuclear current operator, i.e.

$$J^\mu = \int \mathrm{d}\boldsymbol{r}\ \overline{\Psi}_f(\boldsymbol{r})\ \hat{\jmath}^\mu\ \exp\{\mathrm{i}\,\boldsymbol{q}\cdot\boldsymbol{r}\}\ \Psi_i(\boldsymbol{r})\ , \tag{3}$$

are calculated with relativistic wave functions for initial bound and final scattering states and with the relativistic expression of the nuclear current operator [11].

The bound state wave function

$$\Psi_i = \begin{pmatrix} u_i \\ v_i \end{pmatrix} \tag{4}$$

is given by the Dirac-Hartree solution of a relativistic Lagrangian with scalar and vector potentials [12, 13].

The ejectile wave function is the eigenfunction of the relativistic potential with a scalar and a vector component, obtained from the analysis of proton-nucleus elastic scattering. The solution of the Dirac equation for the scattering state is calculated by means of the direct Pauli reduction method. The Dirac spinor

$$\Psi = \begin{pmatrix} \Psi_+ \\ \Psi_- \end{pmatrix} \tag{5}$$

is written in terms of its positive energy component Ψ_+ as

$$\Psi = \begin{pmatrix} \Psi_+ \\ \frac{\boldsymbol{\sigma}\cdot\boldsymbol{p}}{E+M+S-V}\ \Psi_+ \end{pmatrix}\ , \tag{6}$$

where $S = S(r)$ and $V = V(r)$ are the scalar and vector potentials for the nucleon with energy E. The upper component Ψ_+ can be related to a Schrödinger-like wave function Φ by the Darwin factor $D(r)$, i.e.

$$\Psi_+ = \sqrt{D(r)}\ \Phi\ , \tag{7}$$

and

$$D(r) = \frac{E + M + S(r) - V(r)}{E + M} \ . \tag{8}$$

The two-component wave function Φ is the solution of a Schrödinger equation containing equivalent central and spin-orbit potentials, which are functions of the scalar and vector potentials S and V and are energy dependent.

The effective Pauli reduction appears more flexible than the direct solution of the Dirac equations for all partial waves. It is in principle exact: the Schrödinger-like equation is solved for each partial wave starting from the relativistic optical potential.

The electromagnetic current operator can be written in a relativistic form with the cc2 definition of Ref. [14], i.e.

$$\hat{j}^{\mu}_{\rm cc2} = F_1(Q^2)\gamma^{\mu} \ + \ {\rm i}\frac{\kappa}{2M}F_2(Q^2)\ \sigma^{\mu\nu}q_{\nu} \ , \tag{9}$$

where $q^{\nu} = (\omega, \boldsymbol{q})$ is the four-momentum transfer, $Q^2 = \boldsymbol{q}^2 - \omega^2$, F_1 and F_2 are Dirac and Pauli nucleon form factors, κ is the anomalous part of the magnetic moment, and $\sigma^{\mu\nu} = {\rm i}/2\ \left[\gamma^{\mu}, \gamma^{\nu}\right]$.

However, if we use the Gordon decomposition, we can obtain two other expressions that are equivalent for an on-shell nucleon, i.e.,

$$\hat{j}^{\mu}_{\rm cc1} = G_{\rm M}(Q^2)\gamma^{\mu} \ - \frac{\kappa}{2M}F_2(Q^2)\ \overline{P}^{\mu} \tag{10}$$

and

$$\hat{j}^{\mu}_{\rm cc3} = F_1(Q^2)\frac{\overline{P}^{\mu}}{2M} + \frac{\rm i}{2M}G_{\rm M}(Q^2)\ \sigma^{\mu\nu}q_{\nu} \ , \tag{11}$$

where $G_{\rm M} = F_1 + \kappa F_2$ is the Sachs magnetic form factor and $\overline{P}^{\mu} = (E + E', \boldsymbol{p} + \boldsymbol{p}')$. In order to fulfill current conservation the initial proton momentum and energy are taken as [14]

$$\begin{aligned} \boldsymbol{p} =& \boldsymbol{p}' - \boldsymbol{q} \ , \\ E =& \sqrt{|\boldsymbol{p}|^2 + M^2} \ , \end{aligned} \tag{12}$$

where $\boldsymbol{p}'$ is the asymptotic value of the outgoing proton momentum.

All these expressions are equivalent for an on-shell nucleon, but they can give different results for an off-shell one, like the initial nucleon in knockout reactions. This can produce ambiguities that can be large when the nucleon is highly off-shell. This is, e.g., the case of photoproduction. Note that we can also obtain an infinite number of equivalent expressions by combining with different weights (normalized to one) the above equations for the current.

The coincidence cross section of the $(e, e'p)$ reaction can be written in terms of four nuclear structure functions [3, 11] by separating the longitudinal and

transverse components of the nuclear current with respect to the momentum transfer. One has

$$\sigma_0 = \sigma_{\rm M}\ E'|\boldsymbol{p}'|\left\{v_{\rm L}R_{\rm L} + v_{\rm T}R_{\rm T} + v_{\rm LT}R_{\rm LT}\cos\alpha + v_{\rm TT}R_{\rm TT}\cos 2\alpha\right\}, \quad (13)$$

where $\sigma_{\rm M}$ is the Mott cross section and α the out-of-plane angle between the electron-scattering plane and the $(\boldsymbol{q}, \boldsymbol{p}')$-plane. The coefficients v depend only on the electron kinematics. The structure functions R are given by suitable combinations of the components of the nuclear current. They can be separated by experiment and therefore provide complementary information.

3.1 Relativistic *v s* Nonrelativistic Results

The comparison between relativistic and nonrelativistic calculations does not simply give all the effects of relativity, because the nonrelativistic model does already contain some relativistic corrections in the kinematics and in the nuclear current through the expansion in the inverse nucleon mass. The comparison is done in order to show up the differences between the two models and to find the limit of validity of the nonrelativistic approach.

The relativistic result at low energy is smaller than the nonrelativistic one, but the shape of the distributions in DWIA and RDWIA are similar up to about 200 MeV [11]. The spectroscopic factors, obtained by scaling the calculated cross sections to the data, are in RDWIA about 10 – 20% larger than in DWIA analyses, and thus closer to theoretical predictions.

This effect is essentially due to the Darwin factor [15] of Eq. (8) and to the typical normalization factor $(E + M)/2E$. They produce a quenching of the calculated cross section by about 15% with a corresponding enhancement of the spectroscopic factor.

The transverse structure function $R_{\rm T}$ shows, at $T_{\rm p}$ = 100 MeV, a reduction of about 15% with respect to the nonrelativistic calculation, which grows up to about 40% at 300 MeV. Only small differences are found for the longitudinal structure function $R_{\rm L}$ at all the considered proton energies. Its size, however, decreases when the energy increases and therefore its contribution to the cross section becomes less important. Large differences are generally found for the interference structure functions $R_{\rm LT}$ and $R_{\rm TT}$.

As the relativistic effects increase with energy, the conclusion is that the nonrelativistic model can be used with enough confidence at energies around 100 MeV, and, with some caution, up to about 200 MeV. A fully relativistic calculation is necessary above 300 MeV. This result is in agreement with the old one of Ref. [16], where the validity of the relativistic corrections to the nuclear current, calculated as an expansion on $1/M$, were discussed and an upper limit of $|\boldsymbol{q}| \sim 600$ MeV/c was stated for the nonrelativistic calculations.

3.2 Comparison with experimental data

The calculations were applied to the ^{16}O$(e,e'p)^{15}$N reaction where a considerable amount of experimental data, at different energies and kinematics, is available, including polarization measurements.

The bound-state wave function is obtained from Ref. [13], where relativistic Hartree-Bogoliubov equations are solved, in the framework of a model where the mean-field approximation is applied to the description of the ground-state properties of spherical nuclei [17]. The outgoing-proton wave function is calculated by means of the relativistic energy-dependent optical potential of Ref. [18], which fits proton elastic scattering data on several nuclei in an energy range up to 1040 MeV. The Dirac and Pauli form factors F_1 and F_2 in the nuclear current are taken from Ref. [19].

A constant ($\boldsymbol{q}$,ω) or perpendicular kinematics and a parallel kinematics are considered. The incident electron energy and the outgoing proton energy are fixed. In the kinematics with constant ($\boldsymbol{q}$,ω), different values of the recoil or missing momentum $p_{\rm m}$, with $\boldsymbol{p}_{\rm m} = \boldsymbol{q} - \boldsymbol{p}'$, are explored by changing the angle of the outgoing proton. In parallel kinematics, where $\boldsymbol{q}$ is parallel or anti-parallel to $\boldsymbol{p}'$, different values of $p_{\rm m}$ are obtained by changing the electron scattering angle, and thus $\boldsymbol{q}$.

Low-energy data are presented in terms of the reduced cross section [3], which is defined as the cross section divided by a kinematic factor and the elementary off-shell electron-proton scattering cross section $\sigma_{\rm cc1}$ of Ref. [14].

In Figure 1 the reduced cross section measured at NIKHEF [20] for the ^{16}O$(e,e'p)$ knockout reaction and for the transition to the 1/2$^-$ ground state and the 3/2$^-$ excited state of ^{15}N are displayed and compared with the results of the relativistic and nonrelativistic calculations.

The relativistic results are lower than the nonrelativistic ones and the corresponding spectroscopic factors are therefore larger than those deduced from nonrelativistic analyses. For $\rm p_{1/2}$ state, e.g., we have 0.70 with RDWIA and 0.65 for DWIA.

Only small differences are found at this proton energy between the two models. The results are almost equivalent in comparison with data, which are reasonably described by both calculations.

In Figures 2 and 3 the cross section and the structure functions measured at TJNAF [8] for the ^{16}O$(e,e'p)$ knockout reaction and for the transitions to the $1/2^-$ ground state of ^{15}N are displayed and compared with the RDWIA results. The structure function $R_{\rm TT}$ was not separated from $R_{\rm L}$, as this can be done only in an out-of-plane kinematics. In any case it is very small. The differences between the different relativistic expressions of the current are small, but nonnegligible at positive missing momenta. This is due to the behavior of the structure function $R_{\rm LT}$ (see Figure 3), which is compensated by $R_{\rm T}$ at negative, but not at positive values of the missing momentum. The agreement with the

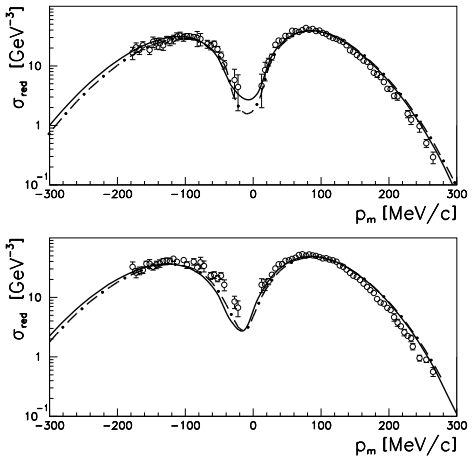

Figure 1. The reduced cross section of the ^{16}O$(e,e'p)$ reaction as a function of the recoil momentum $p_{\rm m}$ for the transitions to the $1/2^-$ ground state (upper panel) and to the $3/2^-$ excited state (lower panel) of ^{15}N, in parallel kinematics with $E_0 = 520$ MeV and $T_{\rm p} = 90$ MeV. The data are from Ref. [20]. The solid lines give the RDWIA result calculated with the cc2 current, the dot-dashed lines the nonrelativistic result.

data is satisfactory. Similar results are obtained for the 3/2$^-$ excited state of ^{15}N.

It is interesting to note that the spectroscopic factor applied to the calculations in Figures 2 and 3 is the same, i.e. 0.70, as that found in the comparison with NIKHEF data shown in Figure 1.

3.3 Polarization Variables

The coincidence cross section for a knocked out nucleon with spin directed along $\hat{\boldsymbol{s}}$, when the electron beam is longitudinally polarized with helicity h, can be written as [3]

$$\sigma_{\rm h,\hat{s}} = \frac{1}{2}\,\sigma_0\,\left[1 + \boldsymbol{P}\cdot\hat{\boldsymbol{s}} + h\Big(A + \boldsymbol{P'}\cdot\hat{\boldsymbol{s}}\Big)\right], \tag{14}$$

where σ_0 is the unpolarized cross section of Eq. (13), $\boldsymbol{P}$ the induced polarization, A the electron analyzing power and $\boldsymbol{P'}$ the polarization transfer coefficient. The polarization directions are: $\boldsymbol{L}$ parallel to $\boldsymbol{p'}$, $\boldsymbol{N}$ along $\boldsymbol{q}\times\boldsymbol{p'}$, and $\boldsymbol{T} = \boldsymbol{N}\times\boldsymbol{L}$. In coplanar kinematics ($\alpha = 0, \pi$), only $P^{\rm N}$, $P'^{\rm L}$, and $P'^{\rm T}$ survive [3].

In Figure 4, the induced polarization $P^{\rm N}$ for the ^{12}C$(e,e'\vec{p})$ reaction [10] is compared with RDWIA calculations. The differences for the three different

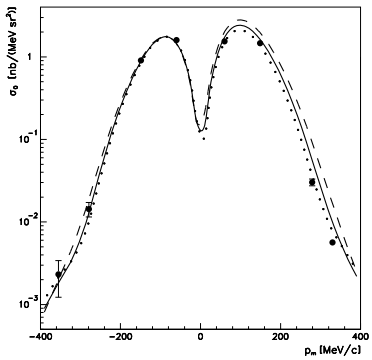

Figure 2. The cross section of the ^{16}O$(e, e'p)$ reaction as a function of the recoil momentum $p_{\rm m}$ for the transition to the $1/2^-$ ground state of ^{15}N in a kinematics with constant $(\boldsymbol{q}, \omega)$, with $E_0 = 2445$ MeV and $T_{\rm p} = 433$ MeV. The data are from Ref. [8]. The solid, dashed, and dotted lines give the RDWIA results with cc2, cc1, and cc3 currents, respectively.

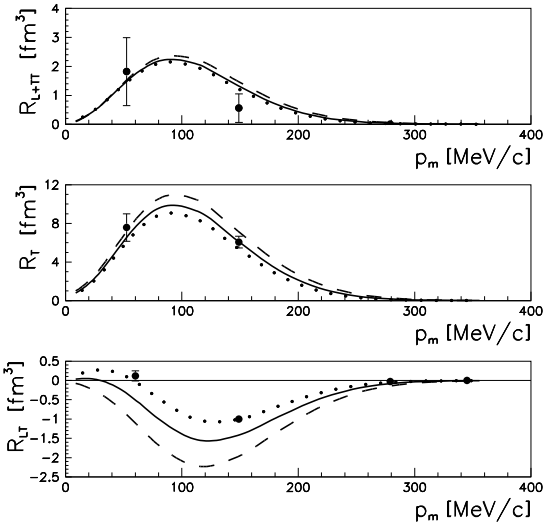

Figure 3. The same as in Figure 2 but for the response functions of the ^{16}O$(e, e'p)$ reaction.

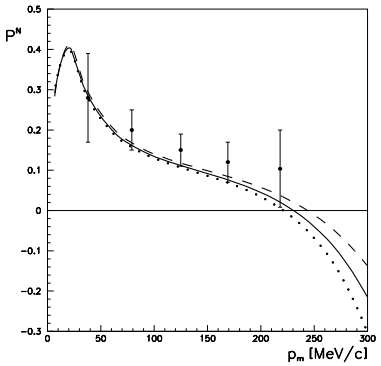

Figure 4. The induced polarization of the emitted proton for the ^{12}C$(e, e'\vec{p})$ reaction as a function of the recoil momentum $p_{\rm m}$ for the transition to the $3/2^-$ ground state of ^{11}B in a kinematics with constant $(\boldsymbol{q}, \omega)$, with $E_0 = 579$ MeV and $T_{\rm p} = 274$ MeV. The data are from Ref. [10]. Line convention as in Figure 2.

expressions of the relativistic current are small at low missing momenta, but become large at higher values.

The components of the polarization coefficient $P'^{\rm L}$ and $P'^{\rm T}$, measured at TJNAF [9] for the ^{16}O$(\vec{e}, e'\vec{p})$ reaction are compared with RDWIA calculations in Figure 5 for $1/2^-$ state. The curves in the figure show the results obtained with the different expressions of the current.

3.4 Photoemission Reactions

The relativistic model was also applied to (γ, p) reactions [21]. In this case the cross section can be written in terms of only one structure function, namely,

$$\sigma_\gamma = \frac{2\pi^2\alpha}{E_\gamma} E' |\boldsymbol{p}'| R_{\rm T} \ . \tag{15}$$

The results are shown in Figure 6 for different photon energies and for the different prescriptions of the relativistic nuclear current. Up to 196 MeV a comparison is also shown with the nonrelativistic calculations. In all the cases the same spectroscopic factor obtained by fitting $(e, e'p)$ data, i.e. 0.70, has been applied.

The different expressions of the relativistic current give large differences. This is mainly due to the fact that the initial proton in (γ, p) reactions is highly off-shell, which makes unreliable the calculation of the initial proton energy and momentum with Eq. (12), as performed in cc1 and cc3 currents. With respect

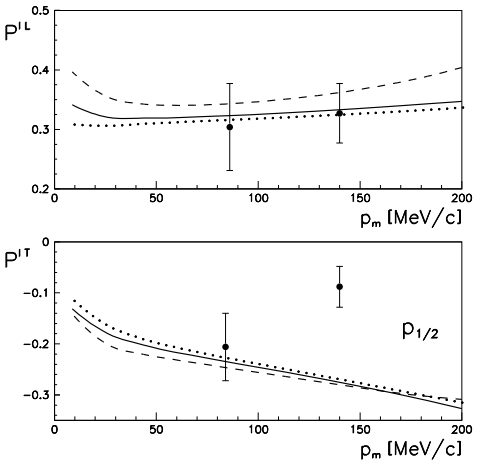

Figure 5. The components of the polarization transfer coefficient P'^{L} and P'^{T} for the ^{16}O$(\vec{e}, e'\vec{p})$ reaction as a function of the recoil momentum p_{m} for the transition to the $1/2^-$ ground state of ^{15}N in the same kinematics as in Figure 2. The data are from Ref. [9]. Line convention as in Figure 2.

to nonrelativistic results, the calculation with cc2 current appears closer to the experimental data, addressing to a smaller contribution of the meson-exchange currents (MEC) in the relativistic than in the nonrelativistic model.

4 Meson-Exchange Current Contributions

The contribution of MEC was evaluated for $(e, e'p)$ and (γ, p) reactions both in the nonrelativistic [26] and in the relativistic model [27].

We assume that the real or virtual photon can interact with a pair of nucleons: one of them is emitted and the other one is reabsorbed. The latter is described by a single particle wave function, taken from the independent particle model. All the particles of the nucleus are involved and their states are assumed to be fully occupied. A more realistic description of these wave functions does not give qualitatively different results.

Taking into account the antisymmetrization of the initial and the final nuclear states and including a correlation function of Jastrow type $f(r_{ij})$, with $r_{ij} =$

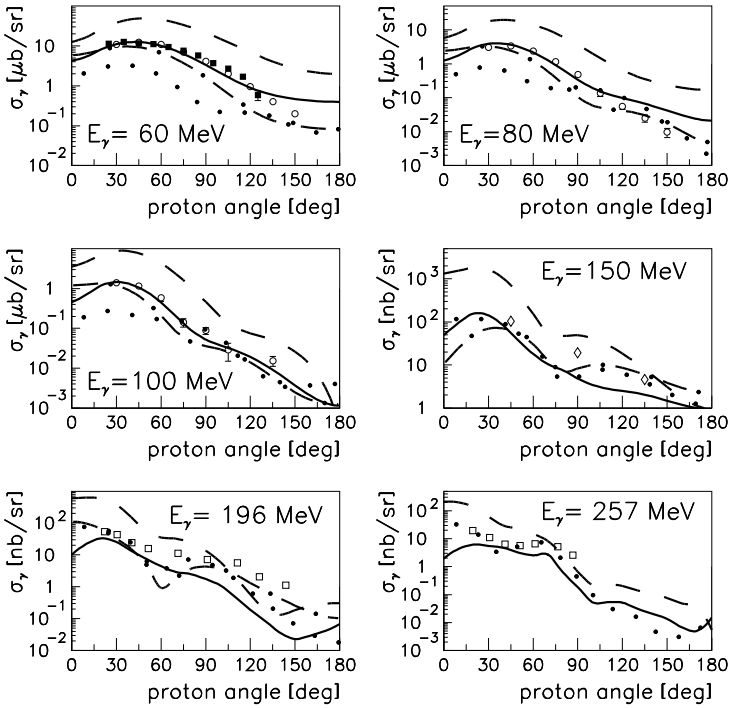

Figure 6. The cross section of the $^{16}\mathrm{O}(\gamma,p)^{15}\mathrm{N}_{\mathrm{g.s.}}$ reaction as a function of the proton scattering angle. The data at 60 MeV are from Ref. [22] (black squares) and from Ref. [23] (open circles). The data at 80 and 100 MeV are from Ref. [23]. The data at 150 MeV are from Ref. [24] and those at 196 and 257 MeV are from Ref. [25]. The results shown correspond to RDWIA calculations with cc2 (solid line), cc1 (dashed line), and cc3 (dotted line) currents. The dot-dashed line is the nonrelativistic result.

$|\boldsymbol{r}_i - \boldsymbol{r}_j|$, the current matrix element can be written as

$$\langle \Psi_{\mathrm{f}} \mid J^{\mu} \mid \Psi_{\mathrm{i}} \rangle \simeq \sum_{\alpha=1}^{\mathrm{A}} \langle \chi^{(-)}(\boldsymbol{r}_1)\varphi_{\alpha}(\boldsymbol{r}_2) \mid j^{\mu}(\boldsymbol{r},\boldsymbol{r}_1,\boldsymbol{r}_2) \mid f(r_{12}) \times (\varphi_{\beta}(\boldsymbol{r}_1)\varphi_{\alpha}(\boldsymbol{r}_2) - \varphi_{\alpha}(\boldsymbol{r}_1)\varphi_{\beta}(\boldsymbol{r}_2))\rangle \ , \quad (16)$$

where where $\chi^{(-)}$ is the distorted wave function of the outgoing nucleon and $\varphi_{\alpha(\beta)}$ are single particle shell-model wave functions.

The current operator can be written as

$$j^{\mu}(\boldsymbol{r},\boldsymbol{r}_1,\boldsymbol{r}_2)=\frac{1}{A-1}\left[J^{(1)\mu}(\boldsymbol{r},\boldsymbol{r}_1)+J^{(1)\mu}(\boldsymbol{r},\boldsymbol{r}_2)\right]+J^{(2)\mu}(\boldsymbol{r},\boldsymbol{r}_1,\boldsymbol{r}_2)\ , \quad (17)$$

where the two-body current contains the lowest-order Feynman diagrams with one-pion exchange. We have thus the seagull and pion-in-flight contributions and the diagrams with intermediate isobar configurations.

While for the $(e,e'p)$ reactions the effect is always small or even vanishing, due to a cancellation between the seagull and the Δ contributions, in (γ,p) it is always large.

First, the results of the nonrelativistic model will be presented. In Figure 7, the cross section for the $^{16}\mathrm{O}(\gamma,p)^{15}\mathrm{N}$ reaction is shown both for the transition

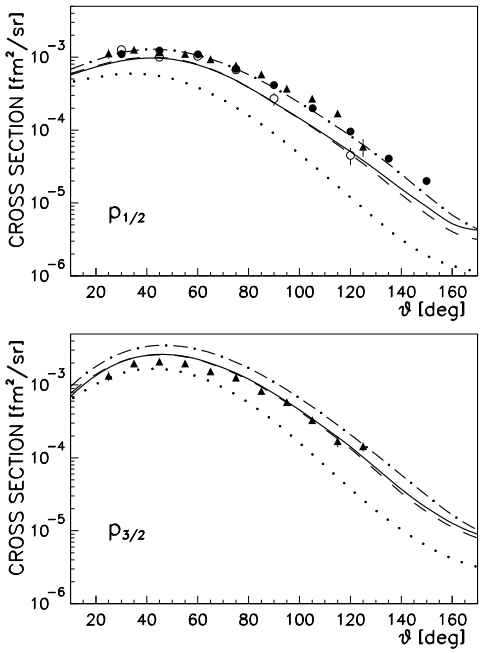

Figure 7. The cross section of the $^{16}\mathrm{O}(\gamma,p)^{15}\mathrm{N}$ reaction as a function of the proton scattering angle at $E_\gamma = 60$ MeV for the transitions to the $1/2^-$ ground state and to the $3/2^-$ excited state of ^{15}N. The experimental data are from [23] (black circles), [28] (open circles) and [22] (triangles). The dotted lines give the contribution of the one-body current. The other lines have been obtained by adding the various terms of the two-body current: one-body + seagull (dot-dashed lines), one-body + seagull + pion-in-flight (dashed lines), one-body+ seagull+ pion-in-flight+ Δ (solid lines).

to the ground state and the excited $3/2^-$ state of ^{15}N. In both cases, the main contribution comes from the seagull term, while the pion-in-flight diagram gives a reduction.

Similar results are displayed in Figure 8 at E_γ = 100 and 196 MeV. The MEC contribution is essential to reproduce the experimental data at E_γ = 100 MeV, while at 196 MeV a discrepancy is found at proton angles higher than $\sim 70^o$, which correspond to values of the recoil momentum higher than 600 MeV/c.

In the relativistic calculation some simplifications have been made. Only the seagull contribution is included and the correlations are neglected.

The results are shown in Figure 9. The effect of MEC is still large, but smaller than in the nonrelativistic model. The experimental data are slightly overestimated, but this can be explained with the expected cancellation due to pion-in-flight diagram. At 196 MeV the experimental data are not reproduced, but at this energy the Δ contribution has an essential role.

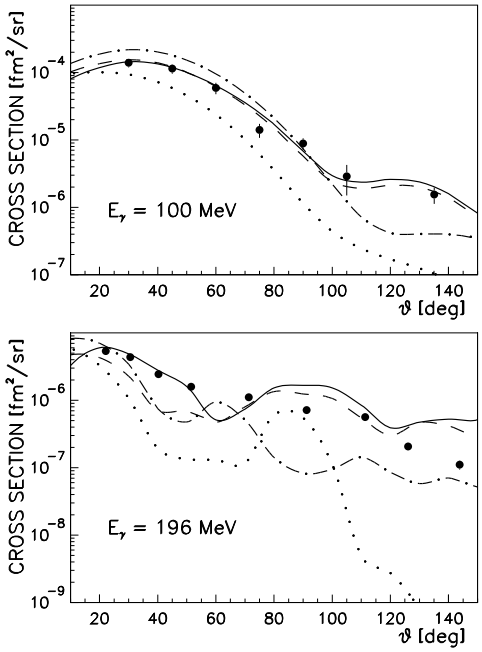

Figure 8. The cross sections of the ^{16}O$(\gamma, p)^{15}$N reaction as a function of the proton scattering angle at $E_\gamma = 100$ and 196 MeV. Line convention as in Figure 7. The experimental data are taken from Refs. [23] ($E_\gamma = 100$ MeV) and [25] ($E_\gamma = 196$ MeV).

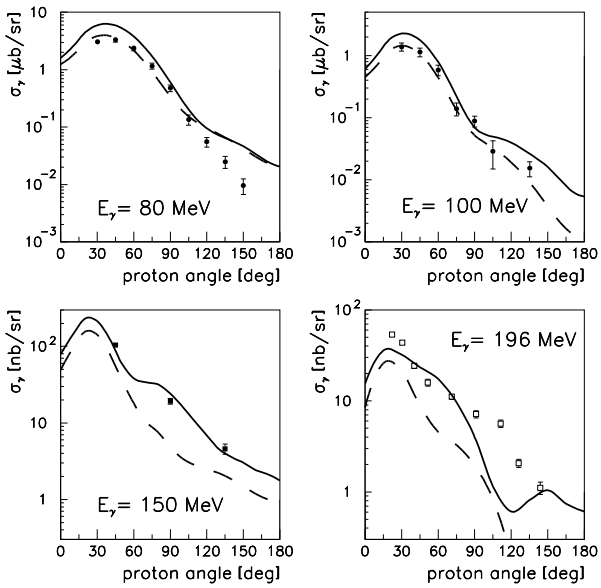

Figure 9. The cross sections for the $^{16}\mathrm{O}(\gamma, p)^{15}\mathrm{N}$ reaction as a function of the proton scattering angle. The dashed line gives the contribution of the cc2 one-body current in RDWIA. Solid line has been obtained adding the seagull contribution. The experimental data are taken from Refs. [23] (E_γ = 80 and 100 MeV), [24] (E_γ = 150 MeV), and [25] ($E_\gamma = 196$ MeV).

5 Conclusions

The cross sections and polarizations for one-proton knockout reactions on ^{16}O are calculated and compared with experimental data. The results given by the relativistic and nonrelativistic models are investigated. They are similar at $T_\mathrm{p} \sim 100$ MeV, but the relativistic ones are smaller and therefore the extracted spectroscopic factors are larger in the relativistic case. The difference increases with energy. The transverse and interference structure functions are particularly sensitive to relativistic effects. A fully relativistic calculation is necessary above $T_\mathrm{p} \sim 300$ MeV. The comparison with experimental data is satisfactory.

In the relativistic calculations there are ambiguities related to the different expressions of the nuclear current, which are equivalent on-shell, but different for an off-shell particle. The effect is small for $(e, e'p)$, but large for (γ, p) reactions. The cc2 current of Eq. (9) should be preferable, because it does not

depend on the initial particle momentum and therefore is more reliable in an off-shell situation.

The contribution of MEC is almost negligible in $(e, e'p)$, but large in the (γ, p) reaction, where it is essential to reproduce the experimental data. In the relativistic approach it is smaller than in the nonrelativistic one, but the final description of the data is comparable.

References

[1] S. Frullani and J. Mougey (1984) *Adv. Nucl. Phys.* **14** 1.

[2] S. Boffi, C. Giusti, and F. D. Pacati (1993) *Phys. Rep.* **226** 1.

[3] S. Boffi, C. Giusti, F. D. Pacati, and M. Radici (1996) *Electromagnetic Response of Atomic Nuclei*, Oxford Studies in Nuclear Physics (Clarendon Press, Oxford).

[4] J. J. Kelly (1996) *Adv. Nucl. Phys.* **23** 75.

[5] J. Mougey *et al.* (1976) *Nucl. Phys. A* **262** 461;
M. Bernheim *et al.* (1982) *Nucl. Phys. A* **375** 381.

[6] P. K. A. de Witt Huberts (1990) *J. Phys. G* **16** 507;
L. Lapikás (1993) *Nucl. Phys. A* **553** 297c.

[7] C. Giusti and F. D. Pacati (1987) Nucl. Phys. **A473** 717; (1988) *Nucl. Phys. A* **485** 461.

[8] J. Gao *et al.* (2000) *Phys. Rev. Lett.* **84** 3265.

[9] S. Malov *et al.* (2000) *Phys. Rev. C* **62** 057302.

[10] R. J. Woo *et al.* (1998) *Phys. Rev. Lett.* **80** 456.

[11] A. Meucci, C. Giusti, and F. D. Pacati (2001) *Phys. Rev. C* **64** 014604.

[12] C. J. Horowitz, D. P. Murdoch, and B. D. Serot (1991) in *Computational Nuclear Physics I: Nuclear Structure*, (ed. by K. Langanke, J. A. Maruhn, and S. E. Koonin; Springer-Verlag, Berlin).

[13] W. Pöschl, D. Vretenar, and P. Ring (1997) *Comput. Phys. Commun.* **103** 217.

[14] T. de Forest, Jr. (1983) *Nucl. Phys. A* **392** 232.

[15] S. Boffi, C. Giusti, F. D. Pacati, and F. Cannata (1987) *Nuovo Cimento A* **98** 291.

[16] C. Giusti and F. D. Pacati (1980) *Nucl. Phys. A* **336** 427.

[17] G. A. Lalazissis, J. König, and P. Ring (1997) *Phys. Rev. C* **55** 540.

[18] E. D. Cooper, S. Hama, B. C. Clark, and R. L. Mercer (1993) *Phys. Rev. C* **47** 297.

[19] P. Mergell, Ulf-G. Meissner, and D. Drechsel (1996) *Nucl. Phys. A* **596** 367.

[20] M. Leuschner *et al.* (1994) *Phys. Rev. C* **49** 955.

[21] A. Meucci, C. Giusti, and F. D. Pacati (2001) *Phys. Rev. C* **64** 064615.

[22] G.J. Miller *et al.* (1995) *Nucl. Phys. A* **586** 125.

[23] D.J.S. Findlay and R.O. Owens (1977) *Nucl. Phys. A* **279** 385.

[24] M. J. Leitch *et al.* (1985) *Phys. Rev C* **31** 1633.

[25] G.S. Adams *et al.* (1988) *Phys. Rev. C* **38** 2771.

[26] C. Giusti and F. D. Pacati (2003) *Phys. Rev. C* **67** 044601.

[27] A. Meucci, C. Giusti, and F. D. Pacati (2002) *Phys. Rev. C* **66** 034610.

[28] F. de Smet *et al.* (1993) *Phys. Rev. C* **47** 652.